

Optimal shape of entrances for a frictionless nanochannel

Christophe Belin, Laurent Joly, and François Detcheverry*

*Univ Lyon, Université Claude Bernard Lyon 1, CNRS, Institut Lumière Matière,
F-69622, Villeurbanne, France*

(Received 5 February 2016; published 19 September 2016)

The nearly frictionless flow of water in narrow carbon nanotubes is a genuine nanofluidic phenomenon with many prospects of applications in membrane technology. When inner dissipation is vanishing, the limiting factor to high flux lies in the viscous dissipation occurring at the tube mouth. As shown by Gravelle *et al.* [Gravelle, Joly, Detcheverry, Ybert, Cottin-Bizonne, and Bocquet, *Proc. Natl. Acad. Sci. USA* **110**, 16367 (2013)], these so-called end effects can be reduced by adding a conical entrance. In this work, we take a step further and search for the optimal entrance shape. We use finite element calculations to compute the hydrodynamic resistance of a frictionless tube with superellipse-shaped entrances and propose an approximate analytical model. If perfect slip applies on its wall, an optimal entrance which is only 10 tube radii in length is sufficient to reduce end effects by an order of magnitude, a performance almost three times better than the optimal cone. In the case of partial slip, the resistance decreases with the entrance length before reaching a plateau at an optimal length controlled by liquid-solid slip. Our results are discussed in connection with biological and artificial systems.

DOI: [10.1103/PhysRevFluids.1.054103](https://doi.org/10.1103/PhysRevFluids.1.054103)

I. INTRODUCTION

Given a body of prescribed volume in a Stokes flow, what is the shape with minimum viscous drag? As established in 1974 by Pironneau, it is axisymmetric with pointed ends, and akin to an American football [1,2]. In this work, we are interested in a similar type of optimal design problem. A frictionless tube is connected at both ends to fluid reservoirs through entrances whose shape may be chosen at will. What is the optimal choice that yields the lowest dissipation and a channel of highest permeability?

Up to the turn of this century, such a question would have been of purely academic interest. Yet, with the recent upsurge in the field of nanofluidics [3–6], it has become apparent that flows at the nanoscale may exhibit behaviors that have no counterpart in the macroscopic realm. Among the new effects uncovered, perhaps the most striking is the nearly frictionless flow of water inside carbon nanotubes (CNTs). First put forward from experiments [7,8], it is now well established in molecular dynamics (MD) simulations. The amount of slip can be quantified by the slip length, which may reach hundreds of nanometers for the narrowest nanotubes [9–12]. Compared to traditional membranes made of organic polymers, membranes based on CNTs would offer a unique combination of properties for water purification, filtration, and desalination [13]. On the one hand, the subnanometric size may ensure the rejection of ions or pollutants by steric or electrostatic hindrance [14], with sieving effects possibly enhanced by tip or core functionalization [15]. On the other hand, the low friction implies that the required pressure—and energetic cost—to maintain the water flow may be much reduced compared to conventional membranes. Accordingly, nanotubes have been touted as the key building block to design the ideal water filter. Though the obstacles on this route are many [16], it is currently under intense investigation [17].

Even if the flow inside the tube is strictly frictionless, forcing the fluid across the membrane nevertheless requires energy. Indeed, the curving of streamlines in the channel entrance and reservoir

*Corresponding author: francois.detcheverry@univ-lyon1.fr

implies that viscous dissipation occurs there, giving rise to “entrance” or “end” effects. For a circular aperture in a zero-thickness membrane, an exact result was given in 1891 by Sampson [18,19], later extended to cylindrical channels with finite length and no-slip boundary condition [20,21]. This condition holds for the vast majority of cases, and unless the channel is very short, with a length comparable to its radius, inner dissipation dominates over entrance effects. For CNTs, however, the situation may be reversed [22–24]. Indeed, a simple estimate for a tube 1 nm in radius and 10 nm in length shows that the entrance contribution outweighs the inner dissipation by a factor of 10: in the overall permeability of the membranes, entrance effects play the leading role.

Can entrance effects be reduced? A first step in this direction was taken recently [25]. Fitting the tube with two cone-shaped vestibules, and choosing the opening angle to its optimal value lying in the range 5° – 25° , the viscous loss was significantly lowered with respect to a plain cylindrical tube. Intriguingly, the predicted hourglass geometry is close to that observed in aquaporins, water-selective biological channels with remarkably high permeability. While conclusions in this first work were based on continuum hydrodynamics, a follow-up study using MD simulations [26] showed that they hold quantitatively, even for the narrowest nanotubes in which water flows in single file. Now, for all its merits, the conical shape is unlikely to be the optimal choice yet, since it includes two angular points, where velocity should vanish, and only a single parameter, the opening angle, is left free to optimize.

The optimal entrance problem requires in principle the optimization of a smooth curve, i.e., an infinite number of degrees of freedom. Sophisticated methods have been developed to do so in the field of optimal shape design [27], with applications from aeronautics to microfluidics [28,29]. A less involved possibility is to consider a family of curves characterized by a small number of parameters. In the minimum drag problem, one can for instance restrict the search to spheroids. It turns out that, compared to Pironneau’s optimal shape, the best prolate spheroid yields an excess in drag that is only 0.1%, suggesting that “optimisation of simple shapes can be effective” in Stokes flow [30]. This “nearly optimal design” is the route that we follow here.

In this work, we explore how the shape of the entrance influences end effects. We examine systematically a three-parameter family of profiles for the entrance, vary its length, and consider perfect or partial slip on its wall. The numerical approach developed in Sec. II is complemented by analytical modeling in Sec. III. We find that a significant improvement is possible with respect to the conical vestibule, with a dissipation that can be more than twice lower. Compared to a plain tube, the reduction in end effects approaches an order of magnitude. Furthermore, we show the existence of an optimal length which is governed by the slip length. Section IV summarizes the implications for natural and man-made nanochannels.

II. NUMERICAL APPROACH

A. Method

We consider an axisymmetric system where an entrance connects a cylindrical tube of radius a to a semispherical reservoir (Fig. 1). The entrance has length L and height H , and its profile is an arc of superellipse

$$h(z) = a + (H - a)\tilde{h}(z/L), \quad (1a)$$

$$\tilde{h}(u) = 1 - (1 - u^{\nu_1})^{1/\nu_2}, \quad (1b)$$

where ν_1 and ν_2 are two exponents controlling the shape of the curve in the vicinity of the tube and reservoir wall, respectively. The conical entrance studied previously [25,26] is recovered for $\nu_1 = \nu_2 = 1$. The two angular points at the tube and reservoir junctions that exist in this particular case disappear as soon as $\nu_i > 1$, replaced by tangential connections. As shown in Fig. 1, different combinations of ν_i exponents allow for a variety of shapes.

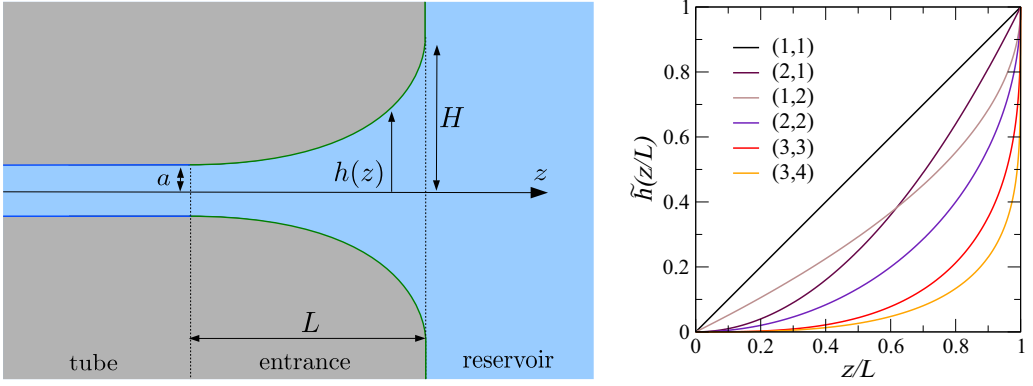


FIG. 1. Left: Geometry of the system. Right: Rescaled profile of the entrance \tilde{h} for various combinations of (v_1, v_2) exponents.

Flows in small scale systems where the Reynolds number is low are described by the Stokes equation

$$\eta \nabla^2 \mathbf{v} = \nabla P, \quad (2)$$

with η the liquid shear viscosity, \mathbf{v} the velocity field, and P the pressure field. In the presence of walls, a boundary condition (BC) must be defined for the velocity field. The standard no-slip BC, $v_{\text{wall}} = 0$, is very robust to describe macroscopic flows, as well as nanoscale flows in the vicinity of wetting walls. However, extensive experimental and numerical work has shown that the no-slip BC can fail at the nanoscale and must be generalized to account for a possible tangential velocity jump at the interface [31–33]. This is the Navier (or partial-slip) BC [34]

$$v_{\text{wall}} = b \left. \frac{\partial v}{\partial n} \right|_{\text{wall}}, \quad (3)$$

where n is the direction normal to the wall and b the slip length, which can be interpreted as the depth inside the solid where the linear extrapolation of the liquid velocity profile vanishes. Equation (3) *a priori* holds only for a flat wall. In the presence of a curved surface, the slip BC must be generalized to tensorial form [35,36]. Denoting by σ the viscous stress tensor and τ the direction tangent to the wall, and equating the viscous stress to a friction stress on the wall proportional to velocity, one gets $\sigma_{\tau n} = \eta v/b$. Introducing the assumption of a Newtonian fluid, one recovers Eq. (3) for a flat wall. An additional term related to curvature may appear on nonflat surfaces. This is not so here, because our system is axisymmetric with no azimuthal component in the flow.

The perfect-slip BC is reached in the limit of infinite slip length, i.e., vanishing liquid-solid friction. This situation is relevant in nanofluidics, where b can be much larger than the channel dimensions, exceeding 100 nm in a CNT with radius below 2 nm [9,10]. Throughout the study, perfect slip is assumed in the tube. The walls of the entrance and reservoir have identical BCs [37], for which we consider several possibilities, ranging from no slip to perfect slip.

The quantity of interest is the hydrodynamic resistance. If a pressure drop ΔP between the reservoir outer boundary and the tube extremity induces a flow rate Q , the hydrodynamic resistance is $R_h = \Delta P/Q$. Below we use the dimensionless resistance defined as

$$\mathcal{R} = \frac{2a^3}{\eta} R_h, \quad (4)$$

where the factor 2 accounts for the two entrances of the channel. Here we assume that the tube is sufficiently long so that the two ends do not interfere, as they are separated by a perfect plug flow in between. A circular pore in an infinitely thin membrane gives $\mathcal{R} = 3$ as shown by Sampson [18].

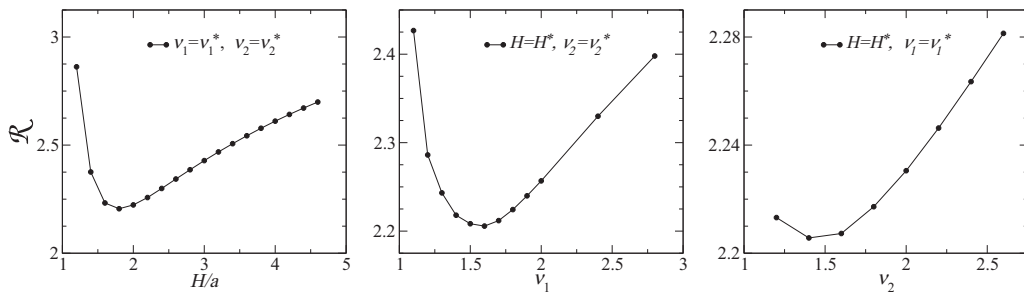


FIG. 2. Global minimum in $\mathcal{R}(H, v_1, v_2)$ for $L = b = a$. The optimal parameters are $H^*/a = 1.8$, $v_1^* = 1.6$, and $v_2^* = 1.4$.

A cylindrical channel with perfect slip on its wall [38] and no entrance yields $\mathcal{R} = \mathcal{R}_0 \simeq 3.8$ [25]. Note that while our results in dimensionless form are valid for any system size, for real systems such as CNTs, the tube radius a would typically be in the nanometer range.

In practice, we solved Eq. (2) using the finite element method with the COMSOL software [39]. We verified that the mesh chosen provides an accuracy below 1% on the measured hydrodynamic resistance. We also tested finite-size effects for the reservoir radius and the tube length, and took sizes ensuring that the results were accurate to a fraction of a percent.

To find the optimal entrance, we systematically varied the three parameters H , v_1 , and v_2 defining the profile. For each entrance length L , a large number of combinations—typically several thousands—were considered. Compared to a gradient-based minimization technique, this systematic exploration is more time consuming but allows for a complete characterization of the $\mathcal{R}(H, v_1, v_2)$ landscape. Whereas one could expect several local minima, we always found a single, global minimum. An example is shown in Fig. 2, where the optimal parameters and resistance are indicated with a star. In a few cases, we observed that resistance values very close to the minimum could be found for parameters that departed substantially from the optimal combination. Though parameter sets differed, the underlying profiles were nevertheless very close to each other [40]. Hence, within the family of curves explored here, the optimal shape was unique.

B. Results

Figure 3 shows how the minimal resistance depends on the entrance length for several slip lengths. If all curves share the same initial decrease from $\mathcal{R} = \mathcal{R}_0$, their subsequent evolutions are very different. For entrances with perfect slip, $\mathcal{R}^*(L)$ exhibits a continuous decrease. The longer the entrance, the lower the resistance. With respect to a conical vestibule, the resistance is significantly reduced, up to a factor of 2.7. With respect to a plain tube, the reduction factor reaches for the longest entrance considered ($L/a = 10$) a value of 8.5. Besides, the monotonic decay of resistance suggests that it vanishes in the limit of long entrances. In contrast, entrances with no-slip BC are never favorable, as they only increase the resistance. Whatever the length, the resistance always subsides upon increasing the height, and the optimal shape is reached in the limit $H \rightarrow \infty$, i.e., in the absence of entrance ($L = 0$).

The intermediate case of finite slip is illustrated in Fig. 3 for the two slip lengths $b = a/10$ and $b = a$. As with $b = \infty$, a steep initial decrease in \mathcal{R}^* is seen for short entrances. However, the resistance subsequently becomes independent of the entrance length. For the two cases considered, the transition length L^* where the plateau is reached is comparable to the slip length. As regards performance, it can be noted that, for short entrances ($L/a < 3$), a superellipse profile with $b = a$ performs better than a conical shape with infinite slip, even though the slip length is modest, being only one tube radius.

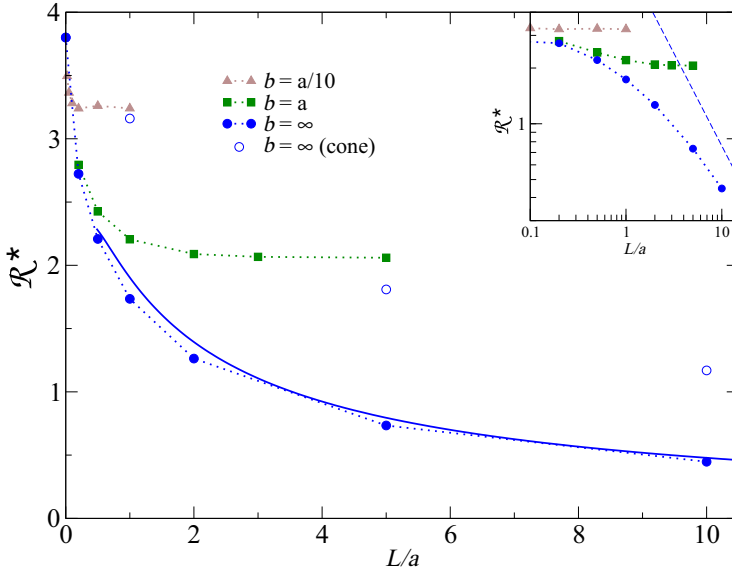


FIG. 3. Optimal hydrodynamic resistance \mathcal{R}^* as a function of entrance length L , for various boundary conditions at the entrance wall. Dotted lines are guides to the eye. The solid line is the model prediction, Eq. (12). The results for optimal conical entrances, taken from Ref. [25], are also shown for comparison. Inset: Same data in logarithmic scale. The dashed line is a power law L^{-1} .

Except for the shortest entrance, the optimal shape, shown in Fig. 4, strongly depends on the BC. For perfect slip, the profile of long tubes includes a gently tapered section, before a rapid widening occurs at the very end. If one considers, to be specific, the point at which the curve slope is unity, it is found close to the abscissa of the reservoir wall. In contrast, the optimal profiles for partial slip with $b = a$ exhibit only weak curvature and, in much of their extent, a slope close to unity. They are reminiscent of a cone geometry with opening angle $\pi/4$. These differences in profile lead to distinct patterns in flow dissipation. Figure 4 presents the map of the local rate of viscous dissipation [19] for three different cases. In the optimal cone with perfect slip, the dissipation is strongly localized in the immediate vicinity of the two angular points [41], with very low values in between. In contrast, dissipation in the optimal superellipse entrance is much more distributed,

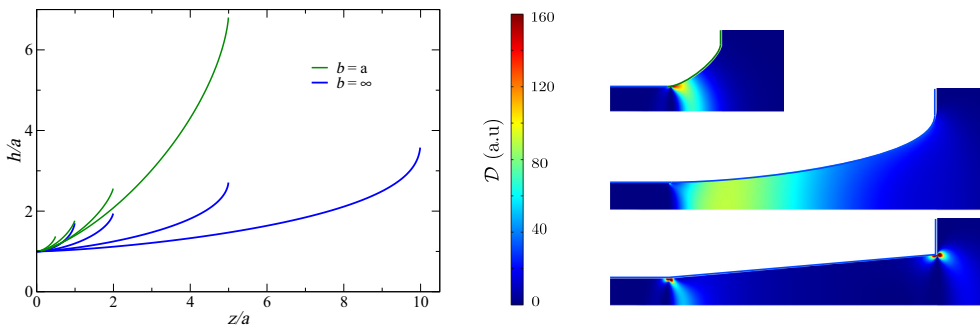


FIG. 4. Left: Optimal entrance profiles for partial and perfect slip and various entrance lengths. For clarity, the reservoir wall is not displayed. Right: Local rate of viscous dissipation, \mathcal{D} (in arbitrary units). From top to bottom, optimal profile for $b = a$ and $L/a = 2$, and optimal profile and optimal cone for $b = \infty$ and $L/a = 10$.

both along the channel axis and in the transverse direction. In the case of partial slip, dissipation is significant throughout the channel as long as the entrance length remains below L^* . For longer entrances, it remains concentrated in the initial portion of the channel and is not very sensitive to the profile in the final portion, since the channel there is already very wide.

III. ANALYTICAL MODEL

An exact analytical approach to our optimal shape problem would require an explicit solution of the Stokes flow for an arbitrary entrance, whose profile should subsequently be optimized. This program can only be carried out numerically. Here we develop an analytical model that captures qualitatively the main phenomena at play. We focus primarily on the case of a long, perfect-slip entrance, which leads to best performance.

A. Perfect slip

When perfect slip holds, the flow in a conical channel is dissipation free, whatever the opening angle α . However, dissipation appears at the connection between two cones with different opening angles. If the angle switches from α_1 to $\alpha_2 > \alpha_1$ at a radius r , an approximate expression for the associated resistance R is

$$R = f(\alpha_2, r) - f(\alpha_1, r), \quad f(\alpha, r) = \frac{C\eta}{r^3} \left[2\alpha + \sin \alpha - \frac{\sin(2\alpha)}{2} \right], \quad (5)$$

with C a numerical constant. Equation (5), which was derived in the supporting information of Ref. [25], is our starting point and the main ingredient of our model. For an infinitesimal change of angle from α to $\alpha + d\alpha$,

$$\frac{dR}{d\alpha} = \frac{C\eta}{r^3} [2 + \cos \alpha - \cos(2\alpha)]. \quad (6)$$

The original derivation yields $C = 1/2\pi$, which severely underestimates the magnitude of resistance [25]. In order to improve the model, we instead adjust C by imposing consistency with the limiting case of a small angle conical entrance, which gives $C = \mathcal{R}_o/4$ [42].

For an entrance with profile $h(z)$, the hydrodynamic resistance may now be written as

$$R[h] = \int_0^L dz F(h, h', h''), \quad F(h, h', h'') = \frac{C\eta}{h^3} \frac{h''}{\mathcal{H}} \left[1 + \frac{1}{\sqrt{\mathcal{H}}} + \frac{2h'^2}{\mathcal{H}} \right], \quad (7)$$

where F is a dissipation (or resistance) linear density, $\mathcal{H} = 1 + h'^2$, the z dependence is implied, and we used $\tan \alpha = h'$. Besides, the entrance profile is assumed to be convex ($h'' \geq 0$). Equation (7) embodies the main phenomenon at work in perfect-slip entrances: curvature in the profile induces dissipation. In the particular case of a cone geometry, $h'' = 0$ and the resistance vanishes as expected.

Variational calculus is now used to minimize the functional $R[h]$. Because the general expression Eq. (7) is intractable, we focus on two limiting cases. In the small slope limit ($h' \ll 1$), one gets $F \sim h''/h^3$, a simple expression that encapsulates the competing requirements in minimizing the resistance. The h^{-3} factor, reminiscent of the Sampson expression, favors enlarging the entrance, but this is only possible with a nonzero curvature, which is penalized by the h'' term. To find the optimal tradeoff, we write the Euler-Lagrange equation

$$\partial_h F - \partial_x \partial_{h'} F + \partial_{xx}^2 \partial_{h''} F = 0, \quad (8)$$

which yields $2h'^2 = h''h$ and the solution

$$h^*(z) = \frac{1}{1 - \kappa z}, \quad \kappa = \frac{1 - H^{-1}}{L}, \quad (9)$$

that satisfies $h(0) = 1$ and $h(L) = H$ [43]. For conciseness, the tube radius a is taken throughout this section as the unit length. Interestingly, the profile h^* yields a local dissipation density $dR/dz \sim \kappa^2$

which is independent of z , implying that the dissipation is uniformly distributed along the channel axis. The entrance resistance in the small slope approximation is then

$$\mathcal{R}^{\text{s.s.}} = \mathcal{R}_0 \frac{(1 - H^{-1})^2}{L}. \quad (10)$$

This contribution increases with H as expected but decreases with L , which is not obvious. Indeed, longer entrances allow for smaller velocity gradient and local dissipation rate, but since the entrance extent is growing at the same time, it is not clear *a priori* which trend will dominate.

In the large slope limit ($h' \gg 1$), one obtains $F \sim h''/(h^2 h^3)$ and the Euler-Lagrange equation $h^{-5} = 0$. While not a well-defined profile, it suggests that resistance here is minimized by a sudden and complete opening of the entrance.

Building on the two limiting cases, we propose to approximate the total resistance of a complete channel (with two entrances) as

$$\frac{\mathcal{R}}{2\mathcal{R}_0} = \frac{(1 - H^{-1})^2}{L} + \frac{1 + \pi - 2h^{*\prime}(L)}{4H^3}. \quad (11)$$

The first term is the small slope contribution taken over the full extent of the entrance, and the second term accounts for the final opening, with the tangent angle switching from $\alpha_1 \simeq h^{*\prime}(L)$, assumed small, to $\alpha_2 = \pi/2$. One must finally fix the entrance height, which has remained a free parameter so far. Minimizing Eq. (11) with respect to H leads to a quadratic equation whose solution is $H^* = (6 + L_1)/10$, where $L_1 = \sqrt{6(6 + 5(1 + \pi)L)}$, and the resistance is finally

$$\mathcal{R}^*(L) = 4\mathcal{R}_0 \frac{5(1 + \pi)(4 + 3L_1)L - 3(6 + L_1)}{L(6 + L_1)^3}. \quad (12)$$

Equation (12) is the main prediction of our model. The resistance is found to decrease monotonically with the entrance length, with in particular $\mathcal{R}^* \sim L^{-1}$ for $L \rightarrow \infty$ [44]. The entrance height grows sublinearly with the length: $H^* \sim L^{1/2}$ asymptotically, suggesting an entrance with ever increasing aspect ratio. Both observations are qualitatively consistent with the numerical results of Sec. II. A quantitative test of Eq. (12) is shown in Fig. 3. In view of the approximations involved, the agreement is quite decent.

To conclude with the perfect-slip case, two remarks are in order. First, while the model seems appropriate only for long entrances, its prediction remains reasonable for length as small as $L = a/2$, below which it breaks down. Second, previous work on the conical entrance had shown that viscous dissipation is localized around the two angular points at reservoir-entrance and entrance-channel connections, and that the resistance was minimal when dissipation was equally divided between the two regions. The superellipse profiles studied here allow for better performance by distributing dissipation more evenly throughout the entrance.

B. Partial slip

Finite slip on the entrance wall introduces a new source of dissipation, which is difficult to account for in general. Here we focus on the case of large slip length. In this limit, the additional dissipation may be treated as an independent contribution evaluated in the lubrication approximation,

$$R^{\text{b}} = \int_0^L dz \frac{8\eta}{\pi h(z)^4} \left(1 + \frac{4b}{h(z)}\right)^{-1}. \quad (13)$$

In effect, the parabolic velocity profile that would be found in a cylindrical tube of infinite extent is assumed to hold locally in each portion of the entrance. For a slip length much larger than the channel radius, the dissipation density scales as $1/bh^3$. Comparing with the curvature expression in the weak slope approximation h''/h^3 , one sees that, at high values, the slip length and the profile radius of curvature play a similar role in the dissipation density.

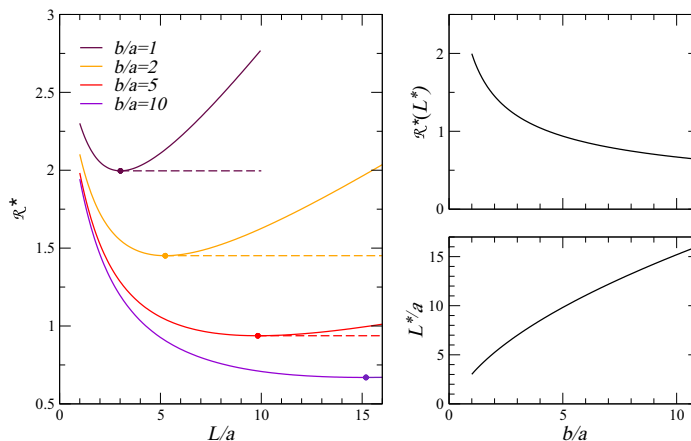


FIG. 5. Model prediction for an entrance with partial slip. Left: The resistance $\mathcal{R}^*(L)$, as given by Eq. (A2), has a minimum indicated by a point at an optimal length L^* , beyond which it is actually constant as explained in the main text (dashed lines). Right: The optimal resistance and entrance length as a function of slip length b .

The curvature-induced resistance at work in the perfect-slip case is minimized for the longest entrances. In contrast, the slip contribution R^b is an increasing function of L , hence favoring short entrances. One can then expect that a balance between those antagonistic trends is reached for an optimal entrance length L^* . To put this qualitative argument on a quantitative basis, one should retrace the steps of Sec. III A. However, adding the new slip contribution yields an Euler-Lagrange equation that appears intractable. Accordingly we resort to a perturbative solution whose expansion parameter is the inverse slip length. As detailed in the Appendix, we again obtain an analytical expression for $\mathcal{R}^*(L)$.

As shown in Fig. 5, the function $\mathcal{R}^*(L)$ now exhibits a minimum at an optimal length L^* . As expected, the larger the slip length, the longer the optimal entrance and the lower the minimal resistance. In the limit of large b , the asymptotic behaviors are $L^* \sim \sqrt{b}$ and $\mathcal{R}^*(L^*) \sim 1/\sqrt{b}$. Besides, it is worth considering the model for moderate values of slip length, even if they fall outside the expected range of validity. For $b = a$, the prediction $L^*/a = 3.0$ is comparable to the numerical result [45], and $\mathcal{R}^*(L^*) = 2.0$ slightly underestimates the exact value 2.2. This suggests that, in spite of its drastic assumptions, the model may be reasonable for modest slip length. Finally, one should note that the increasing branch of the function $\mathcal{R}^*(L)$ is suboptimal. Indeed, a better profile for $L > L^*$ can be constructed by complementing the profile obtained at L^* with a line joining the $z = L$ abscissa at a very large height. In the limit $H \rightarrow \infty$, the resistance is $\mathcal{R}^*(L^*)$. Consistent with the plateau observed in the numerical simulations, the function $\mathcal{R}^*(L)$ is therefore constant beyond the optimal length. Overall, the trends induced by a finite slip can be rationalized within our simple model.

IV. CONCLUSION

We have sought the entrance shape that would most reduce end effects for a frictionless channel. Our findings from numerical and analytical approaches can be summarized as follows: (i) For entrances with partial slip, an optimal length exists, which is controlled by the slip length. (ii) In the case of perfect slip, the resistance can be made arbitrarily small upon increasing the entrance length. (iii) The best performance is reached by distributing evenly the local dissipation along the entrance. Though the physics is completely different, the optimal shape in the perfect-slip case, with a long gradual bore increasing and a sudden opening, is akin to the bell of a trumpet.

We can now come back to the case of aquaporins studied in Ref. [25]. Assuming that the continuum description of the Stokes equation is appropriate and that the profile is designed solely to minimize end effects, the conical vestibule is not the optimal choice for aquaporin channels.

This points to other factors coming into play, such as structural constraints or their function as a water filter. In view of the Stokes flow reversibility, the asymmetry between their two entrances actually gives a hint that the shape is not governed exclusively by resistance minimization. However, it remains instructive, assuming hydrodynamics alone is at play, to identify the optimal shape in a variety of biological systems, be they channels, projectiles, microswimmers, or anguilliform fishes [46–48]. Three decades after Pironneau presented his solution to the minimum-drag problem, the optimal shape and its extension to finite Reynolds number were identified in fungal spores, where it serves to maximize ejecting speed and optimize dispersal [46]. As regards artificial nanochannels and potential use in a sieving membrane, let us consider for concreteness a CNT 1 nm in radius. If optimal, an entrance with length 10 nm would decrease end effects by almost an order of magnitude. There is thus considerable prospect for improvement.

This work may be extended in several directions. First, the possibility of a genuine shape optimization remains, leading the true optimal resistance to which present results are higher bounds. Second, rather than the single channel studied here, one could consider membranes with densely packed tubes and the collective effect arising from hydrodynamic interactions [49]. Third, given the focus on nanofluidic systems, one may take for a starting point the extended Navier-Stokes equation, which includes rotational degrees of freedom while still relying on a continuum description [50]. Finally, experiments probing the influence of entrance shape in biological channels or artificial systems would be of definite interest. Of course, even with state-of-the-art techniques, fine-tuning the entrance profile of nanotubes at the subnanometric level is beyond current capabilities. Almost two centuries passed by before the perfect-slip BC became relevant for water flows. Given the pace of progress in nanopore technology [51], it may not be so long before optimal entrances might actually be realized.

APPENDIX: PERTURBATIVE SOLUTION IN INVERSE SLIP LENGTH

Here we treat the partial slip situation, within the weak slope approximation and in the limit of large slip. The dissipation density is now $F \sim (h'' + 2\epsilon)/h^3$, where $\epsilon = 1/(2\pi Cb)$ is the small parameter. The Euler-Lagrange equation $2h^2 = h''(h + \epsilon)$ is solved perturbatively by seeking an expansion of the form $h = h_o + \epsilon h_1 + \dots$, where the zero-order solution is given by Eq. (9). Repeating the steps above, one finds at first order in ϵ

$$H^* = \frac{6 + L_1}{10} + \epsilon L^2 \frac{672 + 37L_1 + 30\tilde{L}}{300L_1}, \quad (\text{A1})$$

where $\tilde{L} = (1 + \pi)L$. Compared to the perfect-slip case ($\epsilon = 0$), the optimal height is increased. For the resistance, one gets

$$\mathcal{R}^*(L) = \mathcal{T}_o + \epsilon \frac{\mathcal{R}_o L}{L_1(6 + L_1)^4} [11472(6 + L_1) + 5\tilde{L}(2(6744 + 521L_1) + 15\tilde{L}(112 + 3L_1))], \quad (\text{A2})$$

where the zero-order term \mathcal{T}_o is given by Eq. (12). The resistance is now increasing for long entrance, with $\mathcal{R}^*(L) \sim L$ for large L , and it exhibits a minimum at intermediate length, as seen in Fig. 5. The optimal value L^* cannot be obtained in closed form in the general case, but it can be estimated at lowest order in ϵ , yielding $L^* = \sqrt{8/\epsilon} \sim \sqrt{b}$ and $\mathcal{R}^*(L^*) \sim 1/\sqrt{b}$.

[1] O. Pironneau, On optimum profiles in Stokes flow, *J. Fluid Mech.* **59**, 117 (1973).

[2] J. Bourot, On the numerical computation of the optimum profile in Stokes flow, *J. Fluid Mech.* **65**, 513 (1974).

[3] G. Karniadakis, A. Beskok, and N. Aluru, *Microflows and Nanoflows: Fundamentals and Simulation* (Springer, New York, 2005).

- [4] R. Schoch, J. Han, and P. Renaud, Transport phenomena in nanofluidics, *Rev. Mod. Phys.* **80**, 839 (2008).
- [5] W. Sparreboom, A. van Den Berg, and J. Eijkel, Principles and applications of nanofluidic transport, *Nat. Nanotechnol.* **4**, 713 (2009).
- [6] L. Bocquet and P. Tabeling, Physics and technological aspects of nanofluidics, *Lab Chip* **14**, 3143 (2014).
- [7] M. Majumder, N. Chopra, R. Andrews, and B. Hinds, Enhanced flow in carbon nanotubes, *Nature (London)* **438**, 43 (2005).
- [8] J. K. Holt, H. G. Park, Y. Wang, M. Stadermann, A. B. Artyukhin, C. P. Grigoropoulos, A. Noy, and O. Bakajin, Fast mass transport through sub-2-nanometer carbon nanotubes, *Science* **312**, 1034 (2006).
- [9] J. A. Thomas and A. J. H. McGaughey, Reassessing fast water transport through carbon nanotubes, *Nano Lett.* **8**, 2788 (2008).
- [10] K. Falk, F. Sedlmeier, L. Joly, R. R. Netz, and L. Bocquet, Molecular origin of fast water transport in carbon nanotube membranes: Superlubricity versus curvature dependent friction, *Nano Lett.* **10**, 4067 (2010).
- [11] S. K. Kannam, B. D. Todd, J. S. Hansen, and P. J. Davis, How fast does water flow in carbon nanotubes? *J. Chem. Phys.* **138**, 094701 (2013).
- [12] K. Ritos, D. Mattia, F. Calabrò, and J. M. Reese, Flow enhancement in nanotubes of different materials and lengths, *J. Chem. Phys.* **140**, 014702 (2014).
- [13] H. G. Park and Y. Jung, Carbon nanofluidics of rapid water transport for energy applications, *Chem. Soc. Rev.* **43**, 565 (2014).
- [14] B. Corry, Designing carbon nanotube membranes for efficient water desalination, *J. Phys. Chem. B* **112**, 1427 (2008).
- [15] A. Alexiadis and S. Kassinos, Molecular simulation of water in carbon nanotubes, *Chem. Rev.* **108**, 5014 (2008).
- [16] J. Liu, G. Shi, P. Guo, J. Yang, and H. Fang, Blockage of Water Flow in Carbon Nanotubes by Ions Due to Interactions between Cations and Aromatic Rings, *Phys. Rev. Lett.* **115**, 164502 (2015).
- [17] R. Das, M. E. Ali, S. B. A. Hamid, S. Ramakrishna, and Z. Z. Chowdhury, Carbon nanotube membranes for water purification: A bright future in water desalination, *Desalination* **336**, 97 (2014).
- [18] R. A. Sampson, On Stokes's current function, *Philos. Trans. R. Soc. A* **182**, 449 (1891).
- [19] J. Happel and H. Brenner, *Low Reynolds Number Hydrodynamics* (Kluwer, Dordrecht, 1983).
- [20] H. L. Weissberg, End correction for slow viscous flow through long tubes, *Phys. Fluids* **5**, 1033 (1962).
- [21] Z. Dagan, S. Weinbaum, and R. Pfeffer, An infinite-series solution for the creeping motion through an orifice of finite length, *J. Fluid Mech.* **115**, 505 (1982).
- [22] T. B. Sisan and S. Lichter, The end of nanochannels, *Microfluid. Nanofluid.* **11**, 787 (2011).
- [23] W. D. Nicholls, M. K. Borg, D. A. Lockerby, and J. M. Reese, Water transport through (7, 7) carbon nanotubes of different lengths using molecular dynamics, *Microfluid. Nanofluid.* **12**, 257 (2011).
- [24] J. H. Walther, K. Ritos, E. R. Cruz-Chu, C. M. Megaridis, and P. Koumoutsakos, Barriers to superfast water transport in carbon nanotube membranes, *Nano Lett.* **13**, 1910 (2013).
- [25] S. Gravelle, L. Joly, F. Detcheverry, C. Ybert, C. Cottin-Bizonne, and L. Bocquet, Optimizing water permeability through the hourglass shape of aquaporins, *Proc. Natl. Acad. Sci. USA* **110**, 16367 (2013).
- [26] S. Gravelle, L. Joly, C. Ybert, and L. Bocquet, Large permeabilities of hourglass nanopores: From hydrodynamics to single file transport, *J. Chem. Phys.* **141**, 18C526 (2014).
- [27] O. Pironneau, *Optimal Shape Design for Elliptic Systems* (Springer-Verlag, Berlin, 1983).
- [28] B. Mohammadi and O. Pironneau, *Applied Shape Optimization for Fluids* (Oxford University Press, New York, 2009).
- [29] M. Zabaranin and A. Molyboha, Three-dimensional shape optimization in Stokes flow problems, *SIAM J. Appl. Math.* **70**, 1788 (2010).
- [30] T. D. Montenegro-Johnson and E. Lauga, The other optimal Stokes drag profile, *J. Fluid Mech.* **762**, R3 (2015).
- [31] C. Neto, D. R. Evans, E. Bonaccorso, H.-J. Butt, and V. S. J. Craig, Boundary slip in Newtonian liquids: A review of experimental studies, *Rep. Prog. Phys.* **68**, 2859 (2005).
- [32] L. Bocquet and J.-L. Barrat, Flow boundary conditions from nano- to micro-scales, *Soft Matter* **3**, 685 (2007).

- [33] A. E. Kobryn and A. Kovalenko, Molecular theory of hydrodynamic boundary conditions in nanofluidics, *J. Chem. Phys.* **129**, 134701 (2008).
- [34] C. Navier, Mémoire sur les lois du mouvement des fluides, *Mem. Acad. Sci. Inst. Fr.* **6**, 389 (1823).
- [35] W. Chen, R. Zhang, and J. Koplik, Velocity slip on curved surfaces, *Phys. Rev. E* **89**, 023005 (2014).
- [36] L. Guo, S. Chen, and M. O. Robbins, Slip boundary conditions over curved surfaces, *Phys. Rev. E* **93**, 013105 (2016).
- [37] If different BCs are chosen for entrance and reservoir walls, the height H is adjusted to favor the most slipping surface. In particular, if perfect and zero slip apply in the entrance and reservoir, respectively, it becomes favorable to increase H without bound. Our choice avoids such an unwanted situation and ensures that H describes only the entrance geometry, not the slipping properties.
- [38] For a tube with no-slip BC, end effects yield a contribution $\mathcal{R} \simeq 3$, to which the inner dissipation should be added [20,21].
- [39] COMSOL Multiphysics® 2015. Version 5.1. COMSOL, Inc., Burlington, MA, USA.
- [40] For instance, almost similar profiles can be obtained by increasing H and v_2 simultaneously.
- [41] In Fig. 4, the highest values of dissipation are not resolved by the color scheme.
- [42] For $\alpha_1 = 0$ and $\alpha_2 = \alpha \rightarrow 0$, one should have $2R = \mathcal{R}_o \sin \alpha \simeq \mathcal{R}_o \alpha$ as shown in Ref. [25]. Matching with Eq. (6) gives $C = \mathcal{R}_o/4$.
- [43] To obtain Eq. (8), we assume that end points have not only prescribed positions but also fixed slopes, the values of which are an outcome of the calculation.
- [44] For the optimal cone, the asymptotic decay is slower with $\mathcal{R}^* \sim L^{-3/4}$.
- [45] The optimal length for $b = a$ cannot be determined accurately from Fig. 3, but it presumably falls in the range $[2a, 3a]$.
- [46] M. Roper, R. E. Pepper, M. P. Brenner, and A. Pringle, Explosively launched spores of ascomycete fungi have drag-minimizing shapes, *Proc. Natl. Acad. Sci. USA* **105**, 20583 (2008).
- [47] A. Vilfan, Optimal Shapes of Surface Slip Driven Self-Propelled Microswimmers, *Phys. Rev. Lett.* **109**, 128105 (2012).
- [48] W. M. van Rees, M. Gazzola, and P. Koumoutsakos, Optimal shapes for anguilliform swimmers at intermediate Reynolds numbers, *J. Fluid Mech.* **722**, R3 (2013).
- [49] K. H. Jensen, A. X. C. N. Valente, and H. A. Stone, Flow rate through microfilters: Influence of the pore size distribution, hydrodynamic interactions, wall slip, and inertia, *Phys. Fluids* **26**, 052004 (2014).
- [50] J. S. Hansen, J. C. Dyre, P. Daivis, B. D. Todd, and H. Bruus, Continuum nanofluidics, *Langmuir* **31**, 13275 (2015).
- [51] C. Dekker, Solid-state nanopores, *Nat. Nanotechnol.* **2**, 209 (2007).